Measurement and prediction of optical turbulence effects as function of altitude in the marine boundary layer

Arie N. de Jong, Piet B.W. Schwering, Peter J. Fritz,
TNO-Defence, Security and Safety, The Hague, The Netherlands

ABSTRACT

The impact of atmospheric turbulence in the marine boundary layer on the performance of ship-borne and coastal optical and infrared surveillance sensors is well known. On the one hand, the detection process may benefit from scintillation of signals from point-like targets at long range, while target identification is hampered by turbulence induced blurring and beam wander. According to the commonly used turbulence model, based on the Monin-Obukhov similarity theory for the marine boundary layer (the so-called bulk model), the structure function for refractive index C_n^2 decreases with altitude. This height dependence of C_n^2 and the associated blurring, scintillation and beam wander, has consequences for the range performance of sensors against incoming small targets. In the paper, predictions of the height-dependence of turbulence, based upon the bulk model, will be given for a number of scenarios from previous measurement campaigns, such as POLLEX and SAPPHIRE. In these experiments, taking place in a variety of weather conditions (e.g. Air-Sea Temperature Difference (ASTD)), images were collected from vertical arrays of sources at long range. In addition imagery was collected of helicopters, acting as point-targets at ranges up-to more than 30 km. The imagery is used to determine turbulence effects, which are compared with the model predictions. The results of this comparison, showing details on the validity of the model, are presented in the paper.

Keywords: turbulence, scintillation, beam wander, optical blurring, marine boundary layer, IRST, coastal surveillance

1. INTRODUCTION

Variation of the irradiance level (called scintillation) at a sensor pupil, produced by small incoming targets at long range, can have a positive effect on the range performance of optical/IR sensors with high frame rate[1]. The reason is the ratio of the maximum and the mean signal level, which is generally a factor 4 or more for ranges around 20 km. An additional bonus may be produced by the refractive gain, occurring in sub-refractive conditions. Former investigations showed [2], that in these cases of targets near the minimum arrival height, strong signal variations can be generated by surface waves. In addition atmospheric air parcels move up and down locally, due to buoyancy effects, resulting in similar phenomena. It was concluded, that turbulence, being the major source of scintillation, is often not the only mechanism, causing signal fluctuations [3]. It is noted that scintillation can lead to reduced sensor performance in the case of low frame rates. For sensor performance-modeling people, the question is relevant, if this scintillation effect is dependent on the altitude of the target. Most of the published vertical profiles of C_n^2 concern data above land, showing a decrease of C_n^2 with altitude [4], [5]. Associated models, such as the Hufnagel-Valley model and the so-called SLAC model [6], are however more dedicated to ground-to-space imaging applications, in stead of horizontal imaging over seas.

In this paper, we will concentrate ourselves on optical paths at low altitude over sea, where atmospheric boundary layers are considerably different from those over land. At sea, solar heating of the surface is much less than for land-conditions, while the variations of the land-surface structure are more complicated. This leads to C_n^2 values at sea, being one or two orders of magnitude less than in terrestrial areas. We have analysed scintillation and blur measurements, taken at two NATO measurement campaigns: POLLEX [7] and SAPPHIRE [8], where sources were located at long range at various low elevations. In addition, scintillation data were collected of a helicopter target, dipping from about 250 feet altitude to sea level at a range up-to more than 30 km. The measured data are compared with model predictions, based upon the Monin-Obukhov (M-O) theory for the marine atmospheric boundary layer, as implemented by Kunz [9] in the EOSTAR programme at TNO. In the M-O theory, atmospheric bulk parameters such as air- and sea temperature, windspeed and relative humidity are used as input. The model is used to calculate the vertical profiles of windspeed, temperature and specific humidity, allowing the calculation of the structure function for the refractive index C_n^2.

Optics in Atmospheric Propagation and Adaptive Systems XII, edited by Anton Kohnle, Karin Stein, John D. Gonglewski,
Proc. of SPIE Vol. 7476, 747609 · © 2009 SPIE · CCC code: 0277-786X/09/$18 · doi: 10.1117/12.830108

In a similar way we used the M-O model for comparison of predicted and measured refraction effects for overseas paths in the Chesapeake Bay [10] and False Bay [11]. The predicted T-profile (temperature and associated refractive index: n) provides an opportunity to calculate the Angle of Arrival (AoA) of long-distance sources (the absolute angle with the geometrical horizon, under which the sources are seen). It was found, that an adaptation of the T-profile, as provided by M-O, is necessary for various atmospheric conditions. Another deviation of the M-O output concerns the prediction of C_n^2 in cases of small ASTD (near neutral condition). The expected dip of more than two orders of magnitude in the C_n^2 value was not found, which is confirmed by the analysis of Potvin [12] on data from the EOPACE aand VAMPIRA measurement campaigns. It is assumed, that the profiles vary along the propagation path, partly because of variations in ASTD. Another problem area for the prediction of C_n^2 exists at low windspeed (<1 m/s), where the value of C_n^2 should drop another order of magnitude. This prediction is the contrary of the results, obtained in False Bay [11]. The results of the data analysis, presented in this paper, should be useful to further evaluate and improve the M-O model predictions.

2. MODEL PREDICTIONS

We start with the prediction of the vertical profile of C_n^2 for a generic sea environment with a windspeed of 3 m/s, a relative humidity of 70% (both given for an altitude of 10 m) and a sea (surface) temperature of 15 °C. The ASTD has been varied between -4 and +4 K. In the M-O calculation scheme, as prepared by Kunz [13], profiles for the windspeed, air temperature and relative humidity are calculated, including turbulence parameters such as roughness length z_0, the friction velocity u_*, the scaling temperature θ_*, the scaling specific humidity q_* and the Obukhov length L (stability parameter). By using a set of empirical functions, the structure functions C_θ^2, C_q^2 and $C_{\theta q}$ for temperature and specific humidity are obtained, which are directly related to C_n^2.

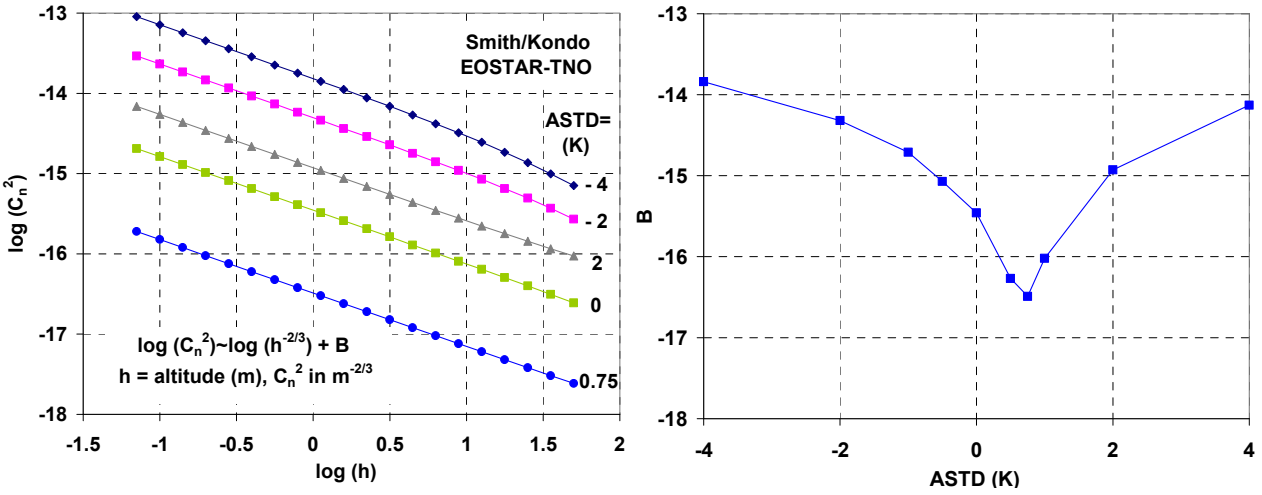

Figure 1. Vertical profiles of C_n^2 versus altitude h for various values of ASTD. The value of the constant B in the relation between log (C_n^2) and log (h) is shown in the plot on the right.

The result of the prediction is shown in Figure 1 for altitudes h above sea level, varying from 0.1 up to 50 m. The plots on the left show for a range of ASTD values a linear relationship between log (C_n^2) and log (h). All slopes have a value of about -2/3, which corresponds to the exponent, given by Beland [14], page 213. The relation: log (C_n^2)=log ($h^{-2/3}$) + B contains a constant B, which depends on the ASTD, as shown in the plot on the right. With the help of this relation, we can calculate the effect of the variations in altitude of an optical beam, for a long optical path over the sea surface, on the scintillation index SI. According to Beland [14], page 185, we use the formula for SI for a plane wave:

$$SI = \sigma_I^2 = 4 * \sigma_\chi^2 = 4 * 0.56 * (2\pi/\lambda)^{7/6} * \int C_n^2 (y) * (L-z)^{5/6} * dz \qquad (1)$$

where the integral runs along the path coordinate z over the total pathlength L. The altitude of the ray y at point z follows from the geometrical relation: $y = h * z/L + h_1 * (L-z)/L - z * (L-z)/2R$, in which h_1 is the receiver altitude and h the source altitude, while R is the radius of the earth ($6.366*10^6$ m). In formula (1), we used a wavelength $\lambda = 0.8*10^{-6}$ m.

Realising that we can write: $C_n^2(y)=10^B * y^{-2/3}$, we have calculated the integral $I = \int y^{-2/3} * (L-z)^{5/6} * dz$ for pathlengths L of 34 and 16 km, receiver altitudes h_1 of 14.5 respectively 7.5 m and an ASTD of -2K (for which the exponent B=-14.3). The integral I is proportional to SI and we find approximately a linear relationship between I and log $(h-h_0)$, where h_0 is the altitude in a vertical plane at the source, for which the optical ray towards the receiver grazes the sea surface. The value of h_0 depends on the sub- or superrefraction, as determined by the ASTD. The plots of I versus log $(h-h_0)$ vary with ASTD. In Figure 2 plots are shown for ASTD values of -2K (B=-14.30), 0K (B=-15.46) and +2K (B=-14.93), which means that we can simply divide the top-curves by factors 13.8 respectively 4.07. In this procedure we have assumed the same value of h_0 for all three cases of ASTD: 30 and 4 m for the ranges of 34 and 16 km. As a result all the three curves in both plots go to the same point Q at the log$(h-h_0)$ axis: absissa x(Q)=1.78 for 34 km and 2.21 for 16 km range.

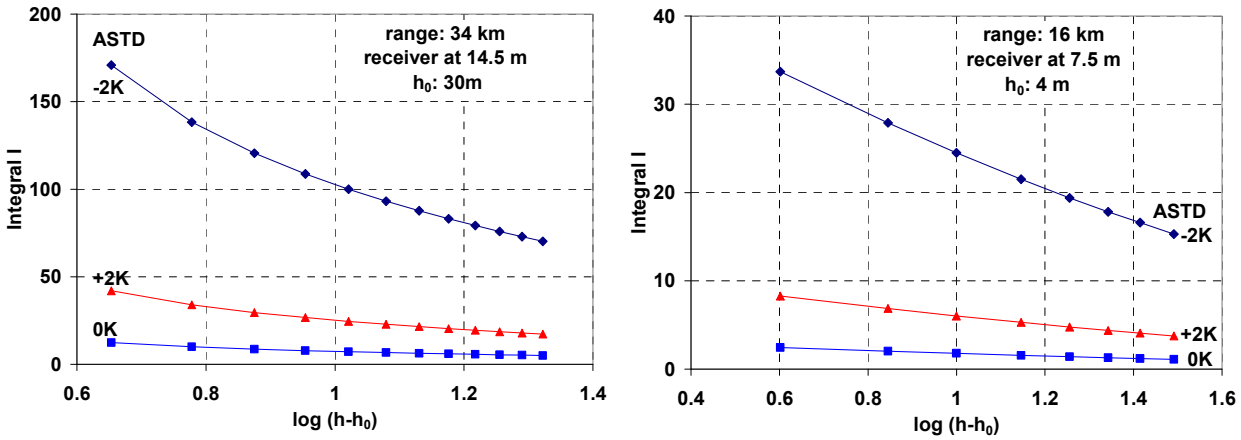

Figure 2. Plots of path-integrated I (proportional to the scintillation index SI) versus log$(h-h_0)$, (h and h_0 in m) for three values of ASTD for ranges of 34 (left) and 16 km (right)

The plots in Figure 2 clearly show a decrease of the SI of more than a factor 2, when the altitude h increases from 34.5 to 51 m for the 34 km range, as well as for the 16 km range, when h increases from 8 to 35 m. In the plots for the 34 km range we observe an additional curling up of SI for the lower altitudes, when the rays are passing the lowest part of the boundary layer (mid-path altitudes smaller than 2 m). The appoximated linear plots, converging to the same point on the log $(h-h_0)$ axis and having different slopes for different ASTD's, allow a simple validation of the M-O theory by means of simultaneous SI measurements on sources at various altitudes. The slopes in Figure 2 for the thee cases of ASTD (respectively -2K, 0K and +2K) are -139.9, -10.14 and -34.38 for the 34 km plots respectively -20.60, 1.49 and 5.06 for the 16 km plots. A major question in this validation process concerns the accuracy of the SI measurements. It is clear, that this accuracy increases with the number of sources and the amount of data. Individual accuracies of 10% or more are preferable when considering the drop-off of SI with altitude. It is noted, that in the predictions, presented here, aperture averaging has not been taken into account. It is assumed however, that this phenomenon, depending on the atmospheric coherence length r_0 and reducing the SI values, occurs in a similar way for all sources at the same range. It is also noted, that variations of the profiles along the range due to variations in windspeed or ASTD, have little effect on the relations between the slopes in Figure 2. It looks as if the presented SI properties are invariant to path-inhomogeneities.

The vertical profile of C_n^2 allows also the evaluation of the decrease of blur with altitude. The blur is specified is in this paper via the atmospheric modulation transfer function MTF(ν), where ν is the spatial frequency (cycles per m) in the focal plane of an optical system with focal length f. According to Beland [14], page 192, MTF(ν) is related to r_0, the wavelength λ and the product fν by:

$$MTF(\nu) = \exp[-\{3.44 * (\lambda f\nu/r_0)^{5/3}\}] \quad \text{with} \quad r_0 = 2.1*\{1.46 * (2\pi/\lambda)^2 * \int C_n^2(y) * dz\}^{-3/5} \qquad (2)$$

The integral in r_0 runs again over the path coordinate z between source and receiver, while the altitude y in $C_n^2(y)$ varies with z. The blur is specified via the cut-off frequency ν_c, at which the MTF is dropped to its 1/e value. The blur in the object plane of the optical system is thus: $1/f\nu_c = 2.1*\lambda/r_0$. The EOSTAR programme directly produces the blur profile for the given atmospheric conditions.

In Figure 3, blur profiles, produced by EOSTAR, are presented for a range of 34.2 km and a receiver altitude of 14.5 km, similar to the geometry used in the previously calculated SI profiles. The blur in microradians (μrad), is presented as function of log ($h-h_0$) for a set of ASTD values. Most of the plots are nearly linear, reason to approximate them by the simple relation: blur = E * log ($h-h_0$) + F. The parameters E and F are also presented in Figure 3 (right), together with the parameter h_0, which slightly varies around 30 m. Again we find, that all linear regression lines through the blur profiles converge to nearly the same point Q on the log ($h-h_0$) axis, which is determined by: log ($h-h_0$) = F/E = 3.1 +/- 0.1. This means that the analysis of SI and blur can be done in a similar way. The plots in Figure 3 (left) show that the blur varies less with altitude than the SI (less than a factor 2). Therefore the blur-measurements have to be more accurate the the SI measurement in order to conclude about the validity of the model concerning profiles of turbulence effects.

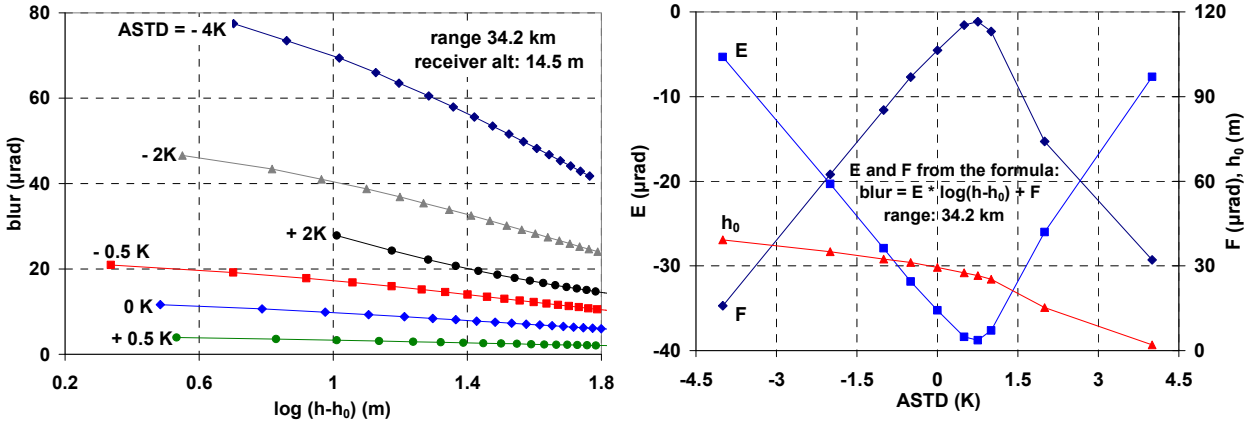

Figure 3. Plots of atmospheric blur as function of log ($h-h_0$) for various ASTD values (left). On the right the values of the approximated slopes E, the blur F at ($h-h_0$)=1m and h_0 are shown as function of the ASTD

3. MEASUREMENT AND ANALYSIS ISSUES

The measurement and analysis of scintillation data requires a considerable amount of care, especially when data are taken over long atmospheric paths by means of imaging sensors. Trivial issues are proper focussing and the avoidance of saturation of the (peak) signals. The best way of focussing is to use an object at shorter range and then turn to the source to be investigated. To avoid saturation, constant monitoring of the maximum signal level is required, taking into account the variations in atmospheric transmission and blurring. It is recommended to use as much dynamic range as possible (preferably more than 8 bits) of the camera system. It is noted here, that sources at long range can produce now and then strong signal bursts, as shown in Figure 4, which should stay within the dynamic range limits.

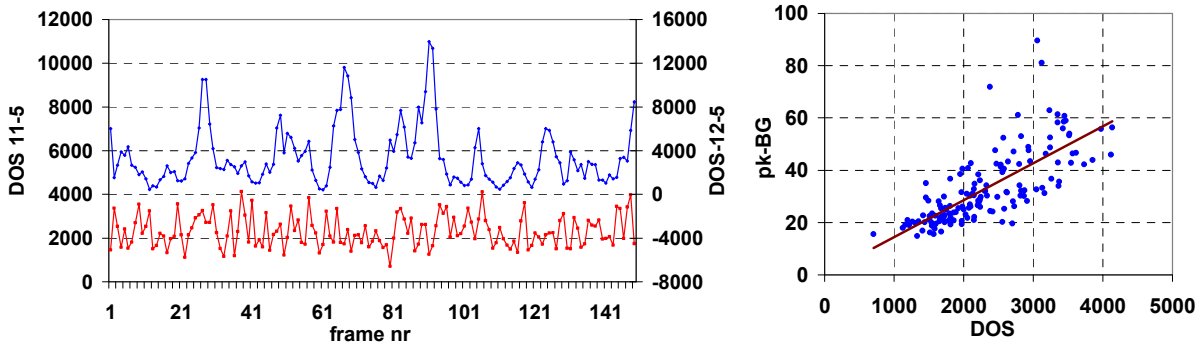

Figure 4. Example of two different types of DOS data for POLLEX source 3 at 34.2 km distance (left). The lower plot has been taken on 11 May 2001 (16:30), the upper "spiky" plot was taken on 12 May (21:47). The scatterplot (right) shows the relation between pk-BG and DOS signals for the 11 May (16:30) data.

It is also important to take care of the radiance of the background near the source and the selection of the spectral band of the camera. In daytime, the background can produce an offset level, creating a considerable reduction of the dynamic range. Sometimes a choice of the direction of view can be made, thus avoiding forward scattering by mid-path aerosols, or reduced background irradiance by the sun can be obtained. In most cases, contrast improvement can be obtained by just using the near-IR band (700-1000 nm). Complete ignorance of background radiance effect is achieved by using a modulated source, such as in the MSRT system [11], which also allows a much larger dynamic range (12 bits). When using a camera system for scintillation measurement, one may choose for two methods to determine the SI value: one is to use the peak signal level compared to the background (called here pk-BG) and the other is to use the total intensity level compared to the background level, integrated over the blur spot (called here Difference of Sums or DOS). It is not trivial that both methods lead to the same SI values, especially when the camera noise can not be neglected and a noise threshold is built into the signal processing procedure. In Figure 4, an example is shown of the relation between the DOS and pk-BG levels for a series of 150 images. In this example the DOS signal levels are found to be 70x stronger than the pk-BG levels. The correlation coefficient, associated with the linear regression line, is found to be 0.74.

It is also noted, that the presence of signal spikes may lead to considerable increase of the SI level. In the two signal recordings, shown in Figure 4, the two SI values for the upper and lower plot are 0.633 and 0.098 respectively, which big difference is mainly due to the presence of spikes. This effect is even stronger if the number of frames in the series is too low or when the frequency of spike-occurrence is low. In comparing the SI levels of sources at different altitudes, one should take care of regularly observing the nature of the signal fluctuations of the various sources and be sure that the signal behaviour of them is similar. In relation to this issue, one should take care of an appropriately long measurement time. A sufficient number of consecutive frames has to be analysed, to be sure that at least one or two spikes (if present) are collected. That means, that at least 50 frames have to be grabbed, preferably more. In our SI analysis we did grab 150 frames, while in the blur analysis about 50-100 frames were collected. Associated to this number of analysed frames is the accuracy of the results. For getting some objective information on this, we analysed for a "normal" signal condition a series of 1200 frames (about one minute of frames) and determined the SI values for subsections of 50 and 150 frames. It appeared, that the required accuracy of 10% (see section 2), was just obtainable with series of 150 frames. For series of 50 frames the accuracy was about a factor 2 less. It is noted, that changes in the transmission- and SI levels may occur in minute time scales due to variations in atmospheric conditions along the path in such periods, as found in [11].

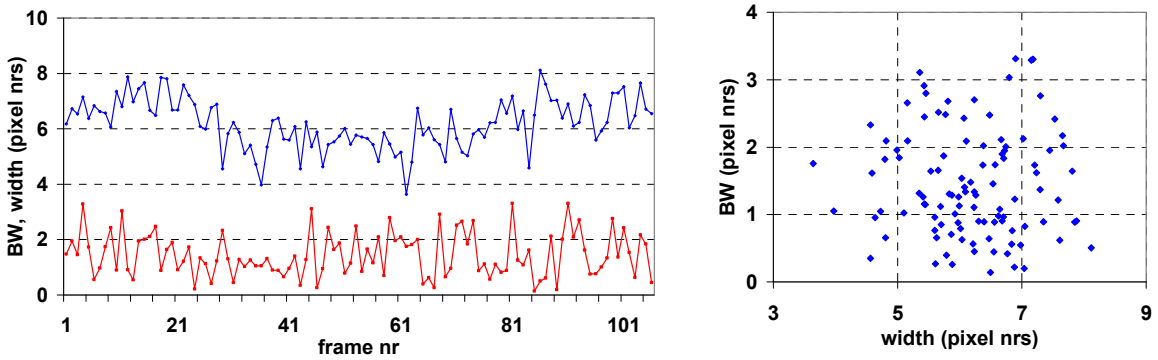

Figure 5. Example of blur measurements on 11 May (18:45): Beam Wander (BW) and width (in pixel numbers) for 106 consecutive frames. On the right a scatterplot of BW and width is shown for this data set.

The analysis of blur was done with series of about 50 frames. For each of the frames the "centres of gravity" x_c and y_c for each of the sources to be analysed, were determined. Via the mean values x_{cm} and y_{cm} for the whole series, the beam wander BW was calculated by means of: $BW=(mean)\{(x_c-x_{cm})^2+(y_c-y_{cm})^2\}^{0.5}$. The width of the blur spot was determined by taking the standard deviation σ_x and σ_y of the pixels in the spot in X and Y direction. For each frame of the series the value of the width $\sigma=(\sigma_x*\sigma_y)^{0.5}$ was calculated and next the mean σ_m for the whole series was obtained. Finally the total blur b_t was calculated by taking into account the camera blur b_c (assumed to be diffraction limited). Realising, that in our case (Celestron camera) a camera pixel corresponds to 6.67 µrad, we defined b_t as: $b_t=2*6.67*(BW^2+\sigma_m^2-b_c^2)^{0.5}$ (µrad) being the blur diameter in the object space. For b_c we took 0.66 pixels (=4.4 µrad). It is noted, that the beam wander and beam width are generally behaving themselves independent from each other, as shown in the example of Figure 5. It was found, that the accuracy of blur measurements, following this method, was generally better than 10%.

4. DATA COLLECTION

From the previous section it is clear that we should be careful in the selection of image data, if quantitative conclusions have to be drawn about the altitude dependence of optical turbulence effects. It appeared, that the data, taken during the POLLEX trials in Livorno (May 2001) and the SAPPHIRE trials near the Chesapeake Bay (June 2006), were suiting our requirements. In addition we could use some helicopter runs, where the helicopter was moving up and down. Several runs were carried out during POLLEX, while a few other runs were obtained during trials near the Netherlands North Sea coast. In the latter case the helicopter was provided with an IR source, simulating a Supersonic Sea Skimming (SSS) incoming missile, hanging 30 m below the helicopter (Figure 6, left). The altitude of the helicopter or source was varied from 25 to 250 ft. During POLLEX and SAPPHIRE an array of vertically and horizontally displaced visible light fixed sources were used. The altitudes of the sources, used in POLLEX and mounted on the island Gorgona, varied from 51.0, 46.6, 42.6, 35.9, 33.0, 30.3, 24.2, 18.8 to 12.4 m above sea level, for sources 1 to 9 (Figure 6 centre). The altitudes of the sources, used in SAPPHIRE and mounted in a mast at Tilghman island were 30.9, 21.4, 13.9 and 5.5 m above sea level for the sources 1 to 4 (Figure 6, right).

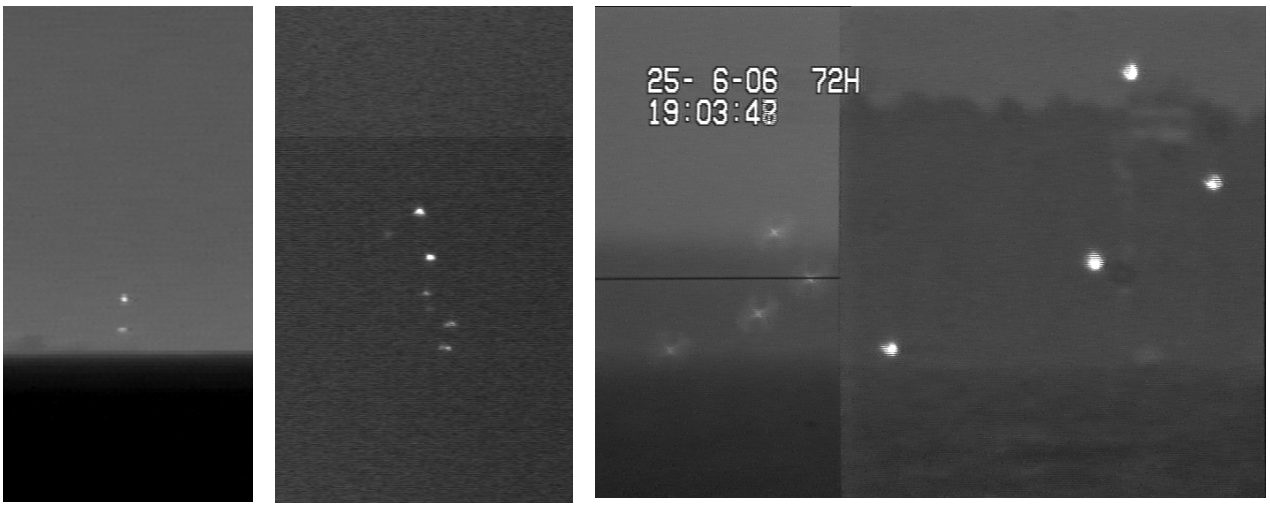

Figure 6. Pictures of sources, of which scintillation and blur were measured as function of altitude; left: a helicopter with IR test source in the North Sea area at 32 km range on 21 January 2003; centre: seven of the nine sources on the island Gorgona at 34.2 km range on 17 May 2001; right: four sources above Chesapeake Bay at 16.2 km range on 25 June 2006 with Theodolite (left) and Celestron (right)

The cameras, used during the collection of the data and important for the investigations, reported in this paper, were:

- **Amber/Raytheon HS** camera, sensitive in the spectral band from 3.0 to 5.0 μm. The lens with a focal length of 250 mm and f/number of 2.5, provided a Field of View of 1.76°x1.76° and a pixel size of 0.12 mrad.
- **Celestron 5'' telescope** with a focal length of 1250 mm and f/number of 10, provided with a Sony XC/73CE CCD camera with a chip size of 4.89x3.64 mm, providing a vertical Field of View of about 2.7 mrad.
- **Topcon AT-G2 theodolite**, provided with a Sony XC/75CE CCD camera with a chip size of 7.95x6.45 mm, and 22.5 mm objective lens. The vertical Field of View was about 6.4 mrad.

The Celestron system was operating in the near IR spectral band (>700 nm), while the theodolite was operating in the visible spectral band. The imagery was recorded on magnetic tape (SVHS or DVcam). During the analysis we used a Matrox Meteor frame grabber, providing series of 150 frames, or a Matlab supported system with series of 50 frames. For each frame series windows were set around each of the sources (separately) to be investigated, together with a background window. Next the operations, providing the SI and/or blur for each series, according to the procedures, described in the previous section, were carried out. During both the POLLEX and SAPPHIRE campaigns, a mid-path buoy was available, providing air- and water temperature and humidity data. Shore-based weather stations provided additional data such as windspeed and solar irradiance. During POLLEX a Canadian station was providing scintillation data along the Mediterranean coast [14].

5. HELICOPTER DATA

For most helicopters the temperatures of the exhaust gases is well controlled to values of about 1000 K. Consequently, the temperatures of the metal parts of the exhaust system is rather stable. The exhaust pipes are thus by far the dominant source of IR radiation. At long ranges (>25 km) the radiation of the gases can be neglected compared to the radiation of the pipes, while the body of the helicopter has a temperature close to that of the ambient air. Furthermore the size of the exhaust is generally rather small (<0.5 m), so we may consider the helicopter as a point source at long range and suitable for investigation of the height dependence of scintillation. From the POLLEX trials we carried out an analysis of four of the runs on 8, 9 and 10 May (range about 31 km) and 17 May (range 25 km). Similarly the data from the North Sea trials were analysed, where we used both the helicopter and the IR source. It was found, that the SI values of both were about the same. In the plots in Figure 7, we just present the variation of SI with altitude for the IR source.

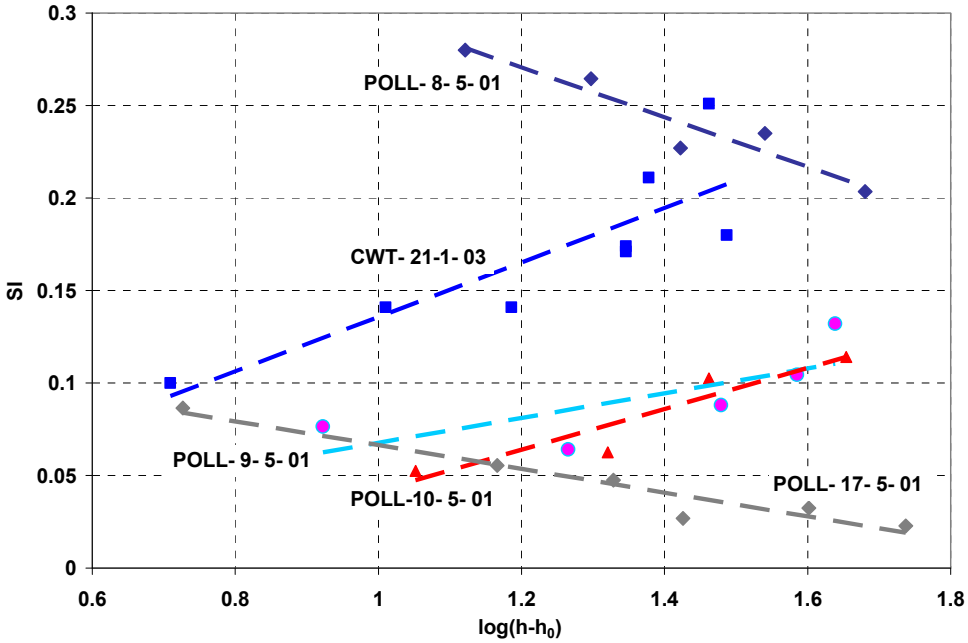

Figure 7. Plots of SI versus log(h-h_0) for helicopter runs during the POLLEX trial Mediterranean Sea (May 2001) and the Cold Weather Trial (CWT) in the North Sea (January 2003)

The plots in Figure 7 show that the SI can both increase and decrease with altitude, and from the weather data, shown in Table 1, no immediate reason for this behaviour can be found. The SI value is obtained via the definition: $SI=(std/avg)^2$, where std and avg are the standard deviation and average of the DOS or pk-BG values of the series of frames. During the POLLEX runs, the ASTD was negative, which implies a slightly unstable boundary layer. All helicopter runs were held in daytime. Looking to the x(Q) values for the runs of 8 and 17 May, we find 3.2 respectively 2.0, which is not far from the expected value of 1.8. It is noted, that by taking SI from equation (1) with $\lambda=4*10^{-6}$ m and assuming a constant C_n^2 along the pathlength of $3*10^4$ m, we get the following relation between SI and C_n^2: $SI=3.37*10^{15}*C_n^2$. A value of SI=0.1 corresponds thus with a C_n^2 value of $3*10^{-17}$ $m^{-2/3}$, which is much less than the value, measured at the shore station.

Table 1. Weather data during the helicopter runs during the POLLEX and CWT trials

Date	Time (UTC)	T air (C)	T sea (C)	ASTD (K)	RH (%)	v wind (m/s)
8-5- 01	11:50	16.1	17.4	-1.3	83	0.5
9-5-01	18:15	17.3	18.5	-1.2	84	2.0
10-5-01	12:09	18.5	19.3	-0.8	76	1.8
17-5-01	09:47	18.9	19.6	-0.7	74	4.7
21-1-03	13:43	7.5	5.0	2.5	81	7.0

6. SAPPHIRE DATA

From the SAPPHIRE imagery, we have analysed 77 series of 150 frames, most of them taken in hours of darkness from 22-29 June. As the lowest source was frequently just above (sometimes chopped by waves) or below the horizon, we did take only scintillation data from the upper three sources. Regression lines were produced through the SI versus log(h-h_0) plots, resulting in slope values, shown together with the SI value for source 2 in Figure 8. The ASTD values, also shown in this figure, shows little correspondence with the SI data. Yet the ASTD correlates rather good with refraction data, as shown in Figure 8 (right), reason to have sufficient confidence in the ASTD values. The slopes generally have negative values, which means a decrease of scintillation with altitude, corresponding to the predictions from the M-O theory.

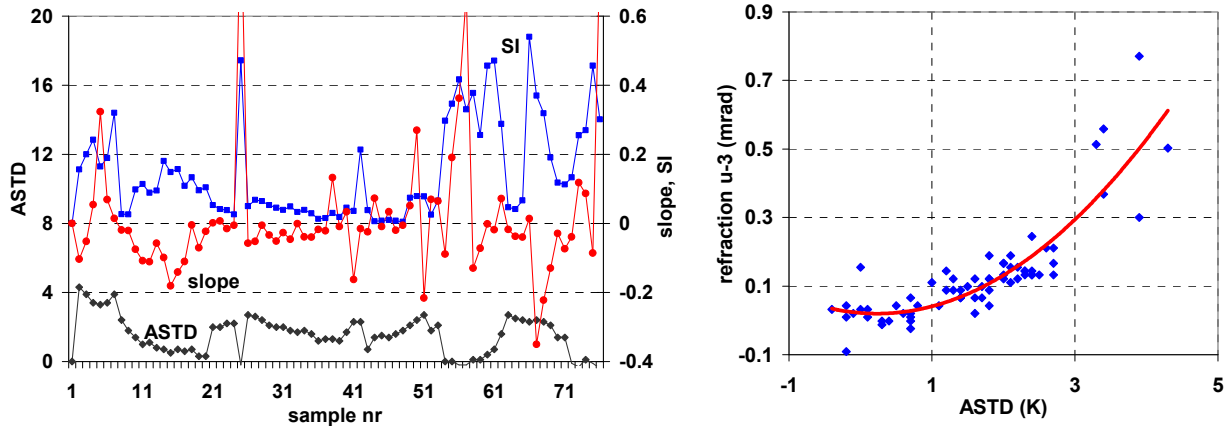

Figure 8. Plots of SI and the slope of the linear regression line of SI versus log(h-h_0) for 77 frame series during the SAPPHIRE trials. Also shown is the ASTD, measured at a midpath buoy (left). The plot on the right shows the relation between the absolute refraction of source 3 and the ASTD.

From the regression lines, their crossing point Q on the log(h-h_0) axis can easily be obtained. These x(Q) values have been plotted for the 77 sample numbers in Figure 9, together with the modeled value of 2.21. We find that in a number of occasions, the measured x(Q) comes close to the predicted value. In a number of other cases however, the slopes have a positive sign, resulting in an increase of scintillation with altitude. A check was made about the value of SI, obtained via the DOS and via the pk-BG method. It was found (see Figure 9, right), that the correspondence of both values was very good with a correlation coefficient of 0.87. Very poor correlation was found between SI and ASTD, as shown in Figure 9 (right), while the smallest SI values (~0.02) were found for an ASTD value around +2K. It is noted, that such SI values over a 16 km path correspond to C_n^2 values of $3.3*10^{-18}$ $m^{-2/3}$ (for $\lambda=0.9*10^{-6}$ m), which is again a very low value.

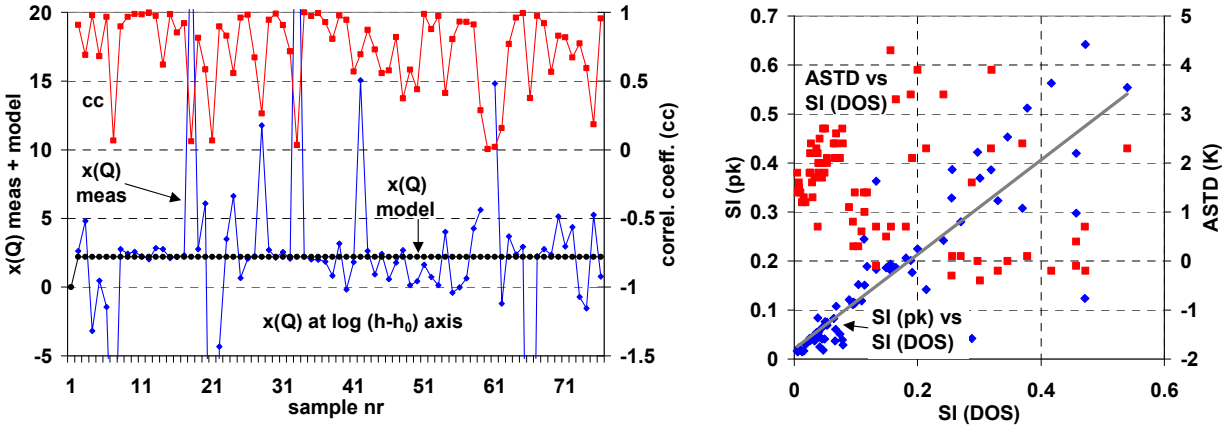

Figure 9. Plot of measured and modeled x(Q) for the 77 series of SAPPHIRE image frames (left). Also shown is the correlation coefficient for the linear regression lines through the SI values of the sources 1, 2 and 3. The plot on the right shows the correlation between SI(pk) and SI(DOS) and ASTD and SI(DOS).

7. POLLEX DATA

From the POLLEX trial, we analysed the SI data for 120 series of 150 frames, spread over the duration of the trial from 4-18 May. Again most of the useful imagery was collected during nighttime, because daytime imagery was threatened by saturation effects. The result of the analysis is shown in Figure 10, together with the slopes of the regression lines for the SI values of three of the sources. Most of the time we selected the sources 1, 3 and 4, but sometimes also the sources 5 or 6 were used instead of source 4. In the same Figure 10 (left), we have plotted the average distortion (defined as the ratio of the measured and real vertical distance between two sources) for the sources 1, 3 and 4. The distortion is a parameter, averaged over the pathlength, contrary to the ASTD, which is a local, midpath parameter. It appears however that ASTD and distortion correlate reasonably well, as shown in Figure 10 (right).

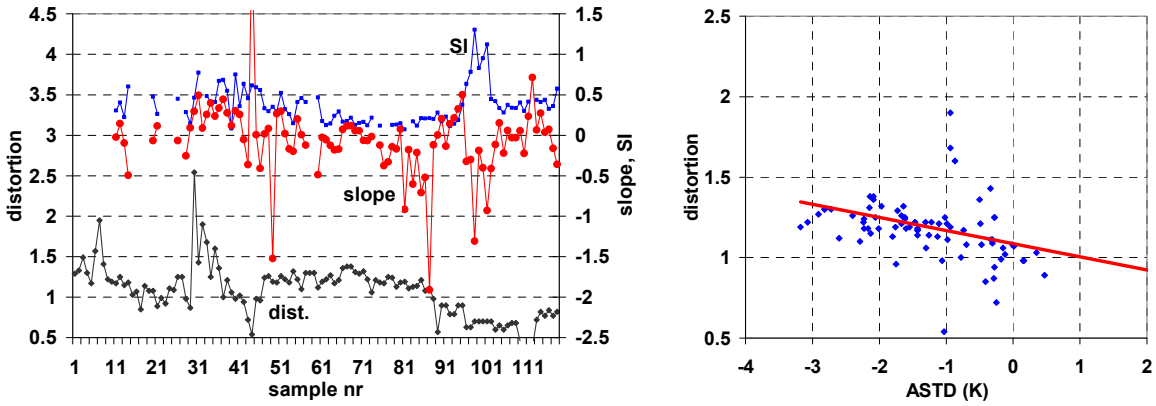

Figure 10. Plots of distortion, SI and slope of the linear regression line through three of the sources on Gorgona for 120 series of frames during the POLLEX trial. Also the relation between the distortion and ASTD is shown (right).

Similar to the previous section, x(Q) was calculated, using the slope data. The results are presented in Figure 11, together with the predicted value of 1.78. We found, that in many cases the agreement is poor; however in a number of cases the agreement is good, most of the time when the correlation coefficient is high. Slope values >0 as well as <0 are found, so scintillation may increase or decrease with altitude. Again a scatterplot between SI(DOS) and SI(pk-BG) (source 3) is presented in Figure 11(right), where we find a poorer correlation and a smaller slope than in Figure 9 for the SAPPHIRE data. Probably for the longer range more anomalies (spikes) are occurring. The same figure contains again a scatterplot between SI(DOS) and ASTD, showing again the absence of any correlation.

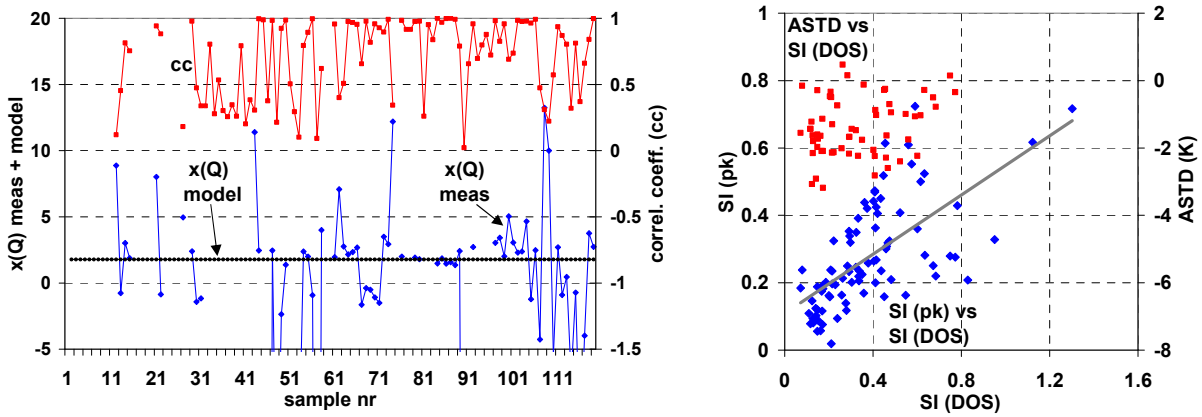

Figure 11. Plots of measured and modeled x(Q) for the 120 series of POLLEX image frames. Also the correlation coefficient for the linear regression lines through the SI values of three of the sources 1, 3, 4, 5 and 6 is shown. On the right, the scatterplot between the SI, obtained via the peak signal and via the DOS method, is shown as well as the scatterplot between SI(DOS) and ASTD.

Finally we present the results of the blur analysis, carried out by following the method, described in Section 3. The blur is plotted for the whole series (all 120 samples) together with the measured and modeled x(Q) in Figure 12. It is noted, that the measured x(Q) values correspond rather good with the modeled value (x(Q)=3.1), while in most cases the blur decreases with altitude. There are however also a large number of occasions, where blur increases or hardly varies with altitude. The correlation coefficient (not shown here), associated with the regression lines through the blur values at the three altitudes, was in 75% of the samples more than 80%, which gives a reasonable feeling of confidence in the trends. In Figure 12 (right) a scatterplot for the blur and SI data for source 3, both obtained through the Matlab analysis system, is shown. The correlation is not so good; it appears, that in various cases the blur decreases with increasing SI values, an effect that we can understand by realising the spiky nature caused by increased interference effects such as one may observe for small, sharply focussed image points. This decrease of blur with increased SI is contrary to the expectation from the equations (1) and (2).

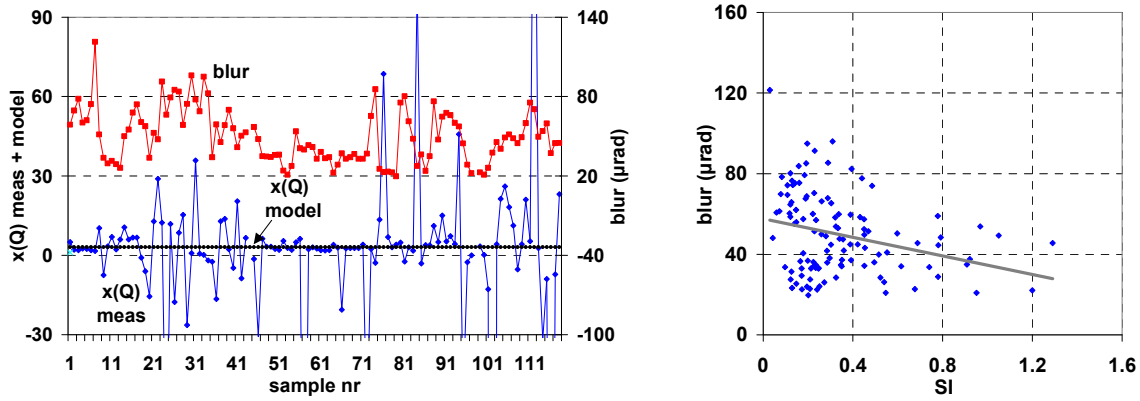

Figure 12. Plot of the blur data (source 3) and the x(Q) values, measured and modeled, for the POLLEX data series. On the right the scatterplot between SI and blur data is shown.

An interesting exercise concerns the calculation of the path averaged C_n^2 value via the measured blur b_t and Scintillation Index SI. For this purpose we return to the formula for the modeled blur: $b_t=1/fv_c = 2.1*\lambda/r_0$, in which one should take for r_0, according to equation (2) $r_0 = 2.1*\{1.46 * (2\pi/\lambda)^2 * \int C_n^2(y) * dz\}^{-3/5}$. When we consider C_n^2 to be constant along the path with length L, we find for b_t for a range L of $34*10^3$ m: $b_t=5.96*10^3*(\lambda)^{-0.2}*(C_n^2)^{0.6}$. By taking for λ: $0.9*10^{-6}$ m and expressing b_t in µrad, we find the following simple relation between C_n^2 and b_t: $C_n^2=(b_t)^{5/3}*0.53*10^{-18}$ ($m^{-2/3}$). For a blur value of 20 respectively 80 µrad we find corresponding C_n^2 values of $0.78*10^{-16}$ and $0.79*10^{-15}$ $m^{-2/3}$. These values for C_n^2 are again smaller than the shore based data. If we introduce a similar simplified relation between C_n^2 and SI (again assuming the plane wave case with a homogeneous C_n^2 along a path of $34*10^3$ m and $\lambda=0.9*10^{-6}$ m): $C_n^2=SI*0.42*10^{-16}$ $m^{-2/3}$.The C_n^2 value, corresponding with SI=0.2, is found to be $0.84*10^{-16}$ $m^{-2/3}$, which is more than the C_n^2 value, found from the blur data; this may well be caused by a certain degree of pupil- and source averaging. The sizes of the pupil (12.5 cm) and source (15 cm) can in the case of small r_0 (<10 cm) lead to reduced SI (and thus C_n^2) values.

8. DISCUSSION AND CONCLUSIONS

In this paper we have presented predictions and measurements of the optical turbulence effects as function of altitude in the marine boundary layer. According to the calculation scheme of Kunz [13], which is based on the Monin-Obukhov similarity theory, we found the C_n^2 to decrease with altitude h via the relation: $C_n^2=10^B*h^{-2/3}$, where B is a constant, depending on the ASTD. The exponent -2/3 does not correspond to the daytime -4/3 value, but is in agreement with the nighttime exponent, given by Beland [4]. With this relation for C_n^2 we calculated the path-averaged and integrated effect of SI and blur for targets at long ranges (16 and 34 km). The altitude dependence of both optical turbulence effects can be approximated by a linear relationship with $\log(h-h_0)$, where h_0 is the altitude in the target plane, where the optical horizon ray intersects. As a consequence of the simple relation between C_n^2 and h, all regression lines through the blur/SI versus $\log(h-h_0)$ plots are crossing the $\log(h-h_0)$ axis at the same point Q with absissa x(Q), independent of ASTD. This invariancy of x(Q) with ASTD can be used to check the validity of the M-O theory and the associated turbulence effects.

Results of SI measurements were presented for runs with helicopters, moving up and down at a range of about 30 km, and for sets of vertically displaced sources (collimated search lights) at ranges of about 16 km (SAPPHIRE) and 34 km (POLLEX). Moreover results of blur measurements were presented for the latter trial. The big question was here if sufficient measurement accuracy could be obtained, in order to perceive the not so strong effect of altitude dependence of both turbulence effects. We did set the accuracy requirement here at 10%, which is a bit rigorous for strong stochastic phenomena as scintillation. It was found that this accuracy level could be obtained for the SI by collecting series of 150 frames. For blur measurements series of 50 frames were adequate, although the standard deviation of the beam wander was bigger than for the beam width. Series of frames had to be selected carefully; for example SI measurements failed in cases of saturation or during the series (lasting 6 to 7 seconds) transmission could change or beam interruption could occur by passing ships. For the helicopter runs, SI measurements could be made for at least five altitudes, allowing an enhancement of the accuracy by taking regression lines through the SI/log(h-h_0) points. For the fixed sources we were able to use SI (and blur) data for three sources, while similarly regression lines were produced. Unfortunately, for most of the daytime imagery, the signals of the CCD camera were saturated, which resulted in a somewhat limited data set.

The slopes of the regression lines provided direct information on the nature of SI/blur increase or decrease with altitude and on the value of x(Q). It was found, that for most of the series of frames, SI and blur decreased with altitude, as theory predicts. In addition we found that there was a preference in these cases for the predicted x(Q) values. On the other hand, for many occasions the opposite effect was found, where SI or blur increased with altitude. The bulk weather parameters, that were simultaneously collected via mid-path buoys and shore-based weather stations, did not give any hint about the reason for such anomalous behaviour. One might think about the presence of low-level inversion layers in some of the nighttime conditions. We did not find any correlation between the SI and ASTD data, where the model predicts a dip in the SI value for an ASTD value of about +0.75K. This effect, also found previously [11], may be caused by variations of ASTD along the path, which was also suggested by Potvin [12]. A somewhat complicating effect did sometimes occur, when low frequency intensity spikes were found, causing enhanced SI values. These spikes, may probably be caused by lensing (refraction) effects in cool air bubbles along the path, as shown in [15]. For the helicopter runs we found in two cases a decrease of SI with altitude and in three cases an increase of SI with altitude.

From the measured SI and blur data, corresponding C_n^2 values were calculated, using the guidelines of Beland [4]. Here we found another deviation from the values, predicted by the M-O based theory. The indirectly measured C_n^2 values were found to be an order of magnitude less than the predictions. But the values were also less than the shore-based data, collected simultaneously, as reported by Forand [16], or more general less than the C_n^2 statistics, given by Weiss-Wrana [17]. There may be a few reasons for finding such low C_n^2 values. Firstly, shore-based C_n^2 measurements, carried out with scintillometers, may suffer from atmospheric transient effects near coastlines. Next, for the long ranges, that we used for our data collection, we may have had problems with atmospheric saturation effects. As pointed out by Andrews [18], the SI can be limited to maximum values of about 1.5. In our data set however, we hardly reached this type of values. Furthermore, we found from both the SI and blur data C_n^2 data, differing not too much. Finally there may have been so-called source and pupil averaging due to small values of the coherence length r_0, compared to the diameter of the source and receiver pupil. Here we note, that for C_n^2 values of 10^{-16} respectively 10^{-17} $m^{-2/3}$, associated r_0 values, taken via equation (2), are 7.8 and 31 cm, which implies, according to Lawrence and Strohbehn [19], limited or no source or pupil averaging. And if there was some averaging effect, it would be similar for all vertically displaced sources.

Another strange effect, that was found by comparing the SI and blur data, concerned their poor correlation. According to equations (1) and (2), the relationship would be: $SI=1.27*10^{-2}*b_t^{5/3}$ for a wavelength of $0.9*10^{-6}$ m and where b_t is given in μrad. So if the blur b_t decreases with altitude, the SI should do that also, which was not the case in most occasions. This effect may be a consequence of neglecting the scintillation effects caused by refraction. Otherwise there may be put a question in our methodology of calculating the total blur by combining the beam wander and beam widths. Possibly we could check this way of SI and b_t interpretation by using the methodology of space-time statistics of the scintillation and displacement fields of the turbulent point-spread function, described by Potvin [20]. In future validation experiments we should preferably use a camera system with higher spatial resolution and larger dynamic range. In connection to this, it would be nice if also daytime imagery could be analysed. One way to overcome this problem, would be a proper choice of the direction of view (compared to the sun-direction). Another possiblity is the use of sources with narrow spectral bands, while providing the camera with a similar band filter. It would be advisable to use more sources at a somewhat smaller range (<15 km) in a taller mast. Finally it would be preferable to perform direct analysis at the measurement location in combination with running a predictive model such as EOSTAR for immediate comparison.

9. REFERENCES

[1] Arie N. de Jong et al, *Enhanced IR target detection by atmospheric effects*, SPIE Volume 4820, Infrared Technology and Applications XXVIII, Seattle, July 2002

[2] Arie N. de Jong et al, *Atmospheric refraction effects on optical/IR sensor performance in a littoral-maritime environment*, Applied Optics, Vol.43, No.34, 1 December 2004

[3] Arie N. de Jong, *Intensity variations of small airborne incoming targets, popping-up above the horizon*, SPIE Volume 5237, Optics in Atmospheric Propagation and Adaptive Systems VI, Barcelona, September 2003

[4] Robert R. Beland, *Propagation through Atmospheric Optical Turbulence*, The Infrared & Electro-Optical Systems Handbook, Volume 2, SPIE Optical Engineering Press, 1993

[5] Larry C Andrews et al, *Near-Ground Vertical Profile of Refractive-Index Fluctuations,* SPIE Volume 7324, Atmospheric Propagation VI, Orlando, April 2009

[6] Larry C. Andrews, *Laser Beam Propagation through Random Media, (page 480)*, SPIE, Bellingham, 2005

[7] Arie N. de Jong et al*, TG16 point target detection experiment POLLEX, Livorno 2001*, SPIE Volume 4820, Infrared Technology and Applications XXVIII, Seattle, July 2002

[8] Karin Stein et al, *The SAPPHIRE trial: Investigations on angular deviation caused by refraction*, SPIE Volume 6747, Optics in Atmospheric Propagation and Adaptive Systems X, Florence, September 2007

[9] Gerard J. Kunz et al, *EOSTAR: an electro-optical sensor performance model for predicting atmospheric refraction, turbulence and transmission in the marine surface layer*, SPIE Volume 5237, Optics in Atmospheric Propagation and Adaptive Systems VI, Barcelona, September 2003

[10] Arie N. de Jong et al, *Refraction Measurements and – modeling over the Chesapeake Bay during the NATO (TG-51) SAPPHIRE trials, June 2006*, SPIE Volume 6747, Optics in Atmospheric Propagation and Adaptive Systems X Florence, September 2007

[11] Arie N. de Jong et al, *Measurement of optical refraction-, transmission- and turbulence effects in the False Bay, South Africa; June 2007*; SPIE Volume 7108, Optics in Atmospheric Propagation and Adaptive Systems XI, Cardiff, September 2008

[12] Guy Potvin et al, *An Empirical Analysis of Bulk C_n^2 Models over Water*, Journal of Applied Meteorology and Climatology, Volume 47, pp. 3044-3060, April 2008

[13] Gerard J. Kunz, *A bulk model to predict optical turbulence in the marine surface layer*, TNO report FEL-96-A053, April 1996

[14] J. Luc Forand et al, *POLLEX trial report, A study of turbulence in the littoral zone*, DRDC Technical Report TR 2004-452, Valcartier, April 2006

[15] Arie N. de Jong, *Geometrical image distortion and aberration for long-range targets in a non-homogeneous atmosphere*, SPIE Volume 5572, Optics in Atmospheric Propagation and Adaptive Systems VII, Gran Canaria, September 2004

[16] J. Luc Forand et al, *C_n^2 estimations at POLLEX*, SPIE Volume 5237, Optics in Atmospheric Propagation and Adaptive Systems VI, Barcelona, September 2003

[17] Karin R. Weiss-Wrana, *Turbulence statistics applied to calculate expected turbulence-induced scintillation effects on electro-optical systems in different climate regions*, SPIE Volume 5891, Atmospheric Optical Modeling, Measurement and Simulation, San Diego, August 2005

[18] Larry C. Andrews et al, *Theory of optical scintillation*, JOSA-A, Vol. 16, No.6, June 1999

[19] Robert S. Lawrence et al, *A Survey of Clear-Air Propagation Effects Relevant to Optical Communications*, Proc. IEEE, Vol. 58, No. 10, October 1970

[20] Guy Potvin et al, *Some theoretical aspects of the turbulent point-spread function*, JOSA-A, Vol. 24, No. 9, September 2007